Computer Assisted Methods in Engineering and Science, **21**: 233–243, 2014.

A meshless method using global radial basis functions for creating 3-D wind fields from sparse meteorological data

Darrell W. Pepper[1], Cody Rasmussen[2], David Fyda[3]

[1] *UNLV, NCACM, Dept. of Mech. Engr., Las Vegas, NV, U.S.A*
e-mail: darrell.pepper@unlv.edu
[2] *Major, USAF, Dept. of Engineering Mechanics, USAFA*

An efficient, global meshless method has been developed for creating 3-D wind fields utilizing sparse meteorological tower data. Meshless methods do not require the need for a mesh in order to connect node points. In this study, node points are placed within the computational domain based on topological features. Wind speeds and directions are obtained from a set of instrumented meteorological towers. Inverse weighting is used to initially establish wind vectors at all nodal points. The Kansa technique, employing global basis functions, is then used to create a mass-consistent, 3-D wind field. The meshless method yields close approximations to results obtained with a high-order finite element technique. The method was implemented using MATLAB.

Keywords: mesh-free method, 3-D wind field, mass-consistent.

1. Introduction

The need for accurate, realistic 3-D wind fields is critically important when encountering issues involving atmospheric releases, assessing wind energy sites and placement of wind turbines, and weather forecasting. However, obtaining sufficient wind data is difficult, costly, and especially problematic when the terrain is complex. Such sparse amounts of data often lead to inaccuracies in depicting and predicting important regional flow features. Reliance on sparse meteorological data in numerical models has been employed for many years, and continues to be a pressing problem

Meteorological models are typically based on conventional numerical methods (e.g., finite difference, finite volume) employing large mesh arrays. These models are commonly run on high-end workstations and supercomputers with massive storage capabilities. In order to accurately resolve regions where topography or high winds exist, a refined mesh is typically required. A finite element model with local mesh adaptation was used by Pepper and Wang [24] to more accurately model atmospheric winds over complex terrain, common to the state of Nevada, USA, at reduced computational cost.

Meshless (also known as mesh-free) methods have become popular for solving problems in applied mechanics and engineering (see [2, 3, 14]. The reasons for their popularity stem from the fact that a computational mesh is not required, programming is simple (allowing models to be run on PCs), and accuracies comparable to higher-order, conventional numerical methods. The placement of nodes within the computational domain can be uniform or randomly scattered; this issue is addressed in greater detail in Gewali and Pepper [10], Choi and Kim [4], and Atluri and Zhu [2].

Efforts to numerically model 3-D wind fields using the governing equations for atmospheric motion have been undertaken by numerous researchers over many years. Examples of such simulations are discussed in Lange [17], Sherman [31], Goodin et al. [11], Pepper [23], Ratto et al. [27],

Finardi et al. [8], Montero and Sanin [21], and Pepper and Wang [25]. However, problems dealing with mesh resolution (resulting in excessive storage requirements) and the inability to accurately resolve terrain hindered many of these early simulations. Even with local mesh refinement techniques used today, such calculations can still become excessive.

In this study, we apply a simple mass consistent approach to minimize the differences between observed (towers) and adjusted (interpolated) nodal values using a meshless method with global radial basis functions. Using USGS Digital Elevation Map (DEM) data for the Nevada Test Site, located near Las Vegas, NV, a nodal pattern is created for the computational domain. Meteorological data recorded in 1993 from 15 towers is used to initialize the wind field. Wind field results from the meshless model are compared with results obtained using an h-adaptive finite element model [24].

2. Mass consistent wind field

The equation for conservation of mass is used to create a diagnostic wind field that is mass consistent. This technique incorporates actual data obtained from meteorological towers to create fixed nodal values at the tower locations. The procedure has been shown to be very effective in establishing micro- and mesoscale wind fields [26]. Early research work on mass consistent models was undertaken by Sherman [31] and later applied by Pepper [23]. The main idea of the technique is to match simulation values with measured meteorological data, using weighted averaging around the sparse data points to fill in values to all the nodes within the computational domain.

Inverse squared weighting ($1/r^2$, where r is the radial distance between the node points and the tower locations) is used to interpolate values to all node points within the computational domain. A fixed radius is used to limit the distance beyond a tower's influence is felt. This technique was used by Goodin et al. [12], Kitada et al. [16], and Pepper [23].

When vertical velocities are either not measured or unavailable, the equation for conservation of mass is used to calculate the vertical velocity, w, based on the divergence correction, i.e.

$$w = -\int_0^z \left(\frac{\partial u}{\partial x} + \frac{\partial v}{\partial y}\right) dz, \tag{1}$$

where u, v, w are velocities in x, y, z directions.

Much of the early work dealing with the generation of 3-D mass-consistent wind fields stems from Lange [17], Sherman [31], and Dickerson [5], who developed the ADPIC pollutant transport model at the Lawrence Livermore National Laboratory. Their model employed an objective analysis procedure using a variational technique first developed by Sasaki [29]. Schaefer and Doswell [30] describes the use of interpolation for creating vector wind fields for atmospheric simulations over regional scales. Warner et al. [33] discusses the accuracy and short comings attributed to the use of observed winds with predicted outcomes. Mathur and Peters [20] later adapted this approach for air pollution modeling. Pepper [23], using a similar approach with finite elements, modeled mesoscale winds over Vandenberg Air Force Base. Ratto el al. [27] gives an overview of these early mass consistent models along with descriptions of the parameters and computational techniques. An improvement to the method was made by Montero et al. [22] using local tetrahedral mesh refinement. In this study, we use the technique from Sherman [31] and Pepper [23] due to its simplicity and easy formulation.

The variance of the difference between an observed (measured) velocity and an analyzed (predicted) velocity can be minimized using an Euler-Lagrange function. This relation was first established by Sasaki [29]. The function is written as

$$E(u,v,w,\lambda) = \int_\Omega \left[\alpha_1^2 (u-u_0)^2 + \alpha_1^2 (v-v_0)^2 + \alpha_2^2 (w-w_0)^2 + \lambda\left(\frac{\partial u}{\partial x} + \frac{\partial v}{\partial y} + \frac{\partial w}{\partial z}\right)\right] d\Omega, \tag{2}$$

where u_0, v_0, w_0 are observed velocity value in x, y, z direction, Ω is physical domain ($d\Omega \equiv dxdydz$), and α_i are Gauss precision moduli where $\alpha_i^2 \equiv 1/(2\sigma_i^2)$. In this approach, the σ_i denote the observation tower errors (i.e., the deviations of the observed field from the desired adjusted field). These moduli are used to account for nondivergence over irregular terrain. Sherman [31] suggested that $(\alpha_1/\alpha_2)^2$ be determined from the magnitude of $(w/u)^2$. This was later employed by Kitada et al. [16] where minimum residual divergence occurred when $(\alpha_1/\alpha_2)^2 = 0.01$. We set $\alpha_1 = 0.01$ (horizontal variation) and $\alpha_2 = 0.1$ (vertical variation). The ratio of α_1/α_2 can be adjusted, if needed.

The corresponding Euler-Lagrange relations that minimize Eq. (2) can be written as:

$$u = u_0 + \frac{1}{2\alpha_1^2}\frac{\partial \lambda}{\partial x}, \tag{3}$$

$$v = v_0 + \frac{1}{2\alpha_1^2}\frac{\partial \lambda}{\partial y}, \tag{4}$$

$$w = w_0 + \frac{1}{2\alpha_2^2}\frac{\partial \lambda}{\partial z}, \tag{5}$$

where λ is the Lagrange multiplier. If Eqs. (3)–(5) are substituted into the continuity equation (assuming constant air density),

$$\frac{\partial u}{\partial x} + \frac{\partial v}{\partial y} + \frac{\partial w}{\partial z} = 0 \tag{6}$$

a Poisson equation can be obtained for $\lambda(x, y, z)$

$$\frac{\partial^2 \lambda}{\partial x^2} + \frac{\partial^2 \lambda}{\partial y^2} + \left(\frac{\alpha_1}{\alpha_2}\right)^2 \frac{\partial^2 \lambda}{\partial z^2} = -2\alpha_1^2 \left(\frac{\partial u_0}{\partial x} + \frac{\partial v_0}{\partial y} + \frac{\partial w_0}{\partial z}\right). \tag{7}$$

Open, or flow-through boundaries, are assumed by setting $\lambda = 0$. When $\partial\lambda/\partial n = 0$, a closed, or no-flow, boundary is assumed.

The application of this simple procedure yields a diagnostic technique based on 15 minute averaged wind velocities. As new meteorological data is obtained, the wind velocities at the towers are updated and a new 3-D wind field is produced. Both Sherman [31] and Dickerson [5] showed that this procedure could produce wind fields that were within a factor of 2 around 50% of the time. Although they used a fairly coarse mesh (compared with today's computational capabilities), the results were impressive. More recent efforts employing localized mesh adaptation significantly improved the results and provided more detailed flow patterns (see [24]).

3. Meshless approach

Traditional numerical methods (e.g., finite difference, finite volume, and finite element) typically require detailed mesh generation. However, a meshless method does not require this initial step. Figure 1 shows the difference in nodal spacing for a meshed vs. meshless approach (using random nodal positioning). Optimal placement of node points is addressed in more detail in Gewali and Pepper [10] and Li et al. [18].

The roots of the development of meshless methods began in the 1970's; however, interest began to develop in the late 1990's for solving applied mechanics problems, and began to see wider use in the 2000's. They have attracted notice for their ease in implementation, compared to the more traditional numerical techniques that rely on a mesh consisting of interconnected node points to calculate values of interest. Although there are a variety of meshless method implementations, most have one property in common: they need not rely on a structured or unstructured mesh (there are some that claim to be meshless, but still rely on a mesh foundation). Strengths of a non-structured

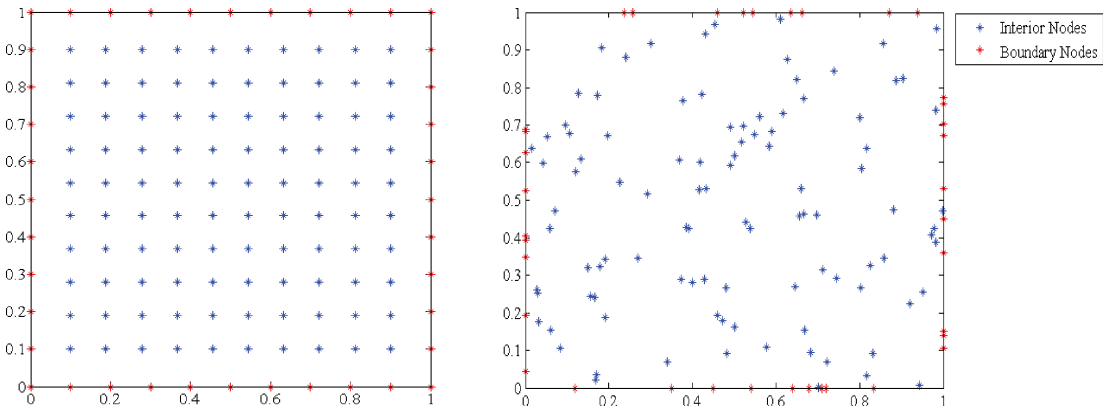

Fig. 1. Structured meshed domain versus meshless domain with random spacing.

mesh become apparent when the problem of complex geometries or time-varying boundaries is considered.

An extensive explanation of the procedure involved in implementing a meshless method is given in Liu [19]. To begin, nodes are placed within the problem domain and on the boundaries. The nodes do not have to be distributed in a uniform manner and can be denser in regions where the greatest changes in variable values occur [10]. Next, shape functions are used to relate the influence of each node to the other nodes in the domain. This is particularly necessary when the nodes are especially unevenly distributed. Shape functions are generally referred to as the support domain for the node of interest with weighted influence. The support domain can take a circular or rectangular shape. The field variable, e.g., U is then interpolated using the displacements at its nodes within the support domain. The shape functions can be used to write a PDE in nodal matrix form, and global matrices can be assembled for the entire problem domain. All that remains is to solve the matrices to obtain solutions to the PDE.

There are various categories of meshless methods. These include smoothed particle hydrodynamics method, reproducing kernel particle method, meshless Petrov-Galerkin method, local radial point interpolation method, finite point method, and the finite difference method with arbitrary irregular grids. Each of the methods has benefits and drawbacks. In this study, radial basis functions were used as this did not require special consideration for nodal placement.

3.1. The RBF method

One of the simplest implementations of a meshless method is the RBF method. Specifically, Kansa's approach [1] is followed in this study. In this method, a basis function relates the influence of surrounding nodes on the node of interest. The nodes closest to the node of interest have the greatest influence. Nodes increasingly farther away have decreasing influence. For example, the distance, d, between radial position, r, can be defined as:

$$d_i = \left[(r - r_i)^2\right]^{1/2}. \tag{8}$$

The most commonly used basis function is the multiquadric (MQ), proposed by Hardy [13]. Other basis functions include Gaussian, thin plate spline, and logarithmic forms (see [34]).

The MQ form has been widely used in constructing approximate solutions to PDEs, and we have elected to use the MQ approach. Upon substitution of the distance formula, the basis function, ϕ, is described as:

$$\phi_j = \left[(r - r_j)^2 + c_j^2\right]^{\beta}, \qquad j = 1, 2...N, \tag{9}$$

where $\beta \equiv 1/2$ and N is the total number of nodes.

Upon defining the domain, Ω, the continuous function $U(x)$ is:

$$U(x) = \sum_{j=1}^{N} \phi_j(x)\alpha_j, \tag{10}$$

where α_j is a series of coefficients. These coefficients must be determined at each continuous function value.

In order to solve partial differential equations (PDEs), we apply a linear operator (L) on the interior, Ω to the continuous function. This gives

$$LU(x) = \sum_{j=1}^{N} L\phi_j(x)\alpha_j. \tag{11}$$

From this relation, the linear operator (the PDE) is applied to the basis function. This requires calculation of the first and second derivatives of the basis functions. PDE's are also subject to boundary conditions. These are taken into account by applying the boundary operator ($\mathcal{B}$) on the boundary $\partial\Omega$ as:

$$BU(x) = \sum_{j=1}^{N} B\varphi_j(x)\alpha_j. \tag{12}$$

By applying a boundary operator, Dirichlet, Neumann, or Robin conditions can be used for the problem.

3.2. Radial-polynomial basis

The use of pure radial functions tends to be inconsistent and so for further accuracy, polynomials added to the basis functions can ensure consistency. However, addition of the polynomials complicates the solution matrices making them difficult to implement. They are, however, accounted for in the following manner:

$$U(x) = \sum_{j=1}^{N} \phi_j(x)\alpha_j + \sum_{k=1}^{M} p_k(x)\gamma_k, \tag{13}$$

where $p_k(x)$ is a polynomial of degree k, and the expansion is subject to the constraint:

$$\sum_{j=1}^{N} p_j(x)\alpha_j = 0. \tag{14}$$

This constraint guarantees unique approximation (see [19]). The interior operator and boundary operator have similar expansions:

$$\begin{aligned} LU(x) &= \sum_{j=1}^{N} L\phi_j(x)\alpha_j + \sum_{k=1}^{M} Lp_k(x)\gamma_k = f, \\ BU(x) &= \sum_{j=1}^{N} B\phi_j(x)\alpha_j + \sum_{k=1}^{M} Bp_k(x)\gamma_k = g. \end{aligned} \tag{15}$$

These are also subject to the constraints:

$$\sum_{j=1}^{N} Lp_k(x)\alpha_j = 0,$$
$$\sum_{j=1}^{N} Bp_j(x)\alpha_j = 0. \tag{16}$$

As stated previously, the addition of polynomials can be beneficial for increasing solution accuracy. It does, however, increase the computation time and complexity of implementation. Also, the solution still relies on well-chosen shape parameters.

3.3. Shape parameters

The shape parameter, c, is critical for determining the accuracy of PDE solutions when applying the radial basis functions. Because of this, careful attention should be given for determining values of the shape parameter. Detailed discussions regarding values for the shape parameter can be found in Fasshauer [6], Franke [9], Hardy [13], and Kansa [15].

Most of the shape parameter formulations rely on the distance, d, and number of nodes, N. Other formulations show a changing shape parameter based on the node position. In summary, the shape parameter can depend on many factors including (see [28]: number and distribution of nodes, the basis function, and computer precision.

Hardy [13] suggested the formulation for the shape parameter, $c = 0.815d$, where d is defined by Eq. (8). Kansa [15] recommended an alternative form where

$$c_j^2 = C_1 \left[1 + C_2(-1)^j\right]$$

with j being even or odd. The parameter, C_1, was defined as the ideal shape parameter for the interior domain and C_2 was used to determine the amplitudes of C_1, depending on whether j is even or odd. In this formulation, $0.25 < C_2 < 0.33$ for the interior values and $0.49 < C_2 < 0.55$ for the boundary values. More detailed discussions regarding the values for c can be found in Fasshauer [7] and Acres [1].

3.4. The Euler-Lagrange equations

To illustrate the application of the meshless method with RBF, Eq. (7) can be expressed as:

$$\nabla^2\lambda = f(\mathbf{x}), \qquad \mathbf{x} \in \Omega,$$
$$\lambda = g(\mathbf{x}), \qquad \mathbf{x} \in \Gamma, \tag{17}$$

where $\mathbf{x} = (x, y, z)$ and $f(\mathbf{x})$ and $g(\mathbf{x})$ denote the divergence of the observed velocity values. Now approximate λ assuming

$$\lambda(\mathbf{x}) = \sum_{j=1}^{N} \phi(r_j)\lambda_j, \tag{18}$$

where r is defined, assuming MQ as the basis function, as

$$\phi(r_j) = \sqrt{r_j^2 + c^2} = \sqrt{(x - x_j)^2 + (y - y_j)^2 + (z - z_j)^2 + c^2}. \tag{19}$$

Likewise, the derivatives can be expressed as:

$$\frac{\partial\phi}{\partial x}=\frac{x-x_j}{\sqrt{r_j^2+c^2}},\qquad \frac{\partial\phi}{\partial y}=\frac{y-y_j}{\sqrt{r_j^2+c^2}},\qquad \frac{\partial\phi}{\partial z}=\frac{z-z_j}{\sqrt{r_j^2+c^2}},$$

$$\frac{\partial^2\phi}{\partial x^2}=\frac{(y-y_j)^2+(z-z_j)^2+c^2}{\sqrt[3]{r_j^2+c^2}},$$

$$\frac{\partial^2\phi}{\partial y^2}=\frac{(x-x_j)^2+(z-z_j)^2+c^2}{\sqrt[3]{r_j^2+c^2}}, \tag{20}$$

$$\frac{\partial^2\phi}{\partial z^2}=\frac{(x-x_j)^2+(y-y_j)^2+c^2}{\sqrt[3]{r_j^2+c^2}}.$$

Substituting into the original equation set, one obtains

$$\sum_{j=1}^{N}\nabla^2\phi(r_j)\lambda_j=f(\mathbf{x}),\qquad i=1,2,\cdots,N_I,$$

$$\sum_{j=1}^{N}\phi(r_j)\lambda_j=g(\mathbf{x}),\qquad i=N_{I+1},N_{I+2},\cdots,N, \tag{21}$$

which produces an $N\times N$ linear system of equations for the unknown λ_j.

3.5. Global versus local RBFs

There are essentially two ways to formulate a meshless approach using radial basis functions: global and local. Each has advantages and disadvantages. The global method, as used in this study, is easy to setup and uses all node points in the domain, but suffers from potential poor conditioning (matrix) and can result in large matrices that need to be efficiently solved. Since our global domain consisted of approximately 625 node points, the global method worked effectively well using simple matrix solution routines found in MATLAB. The local method, which uses only those nodes surrounding the point of interest, requires only small matrices to be inverted per node point, and eliminates the ill-conditioning problem. However, one must repeatedly solve these series of small linear equations. Discussions regarding the use of both approaches is given in Trobec et al. [32], Yao et al. [35], and Waters and Pepper [34].

4. Simulation results

The Nevada Test Site (NTS) was established in 1950 as the United States' nuclear weapons testing area. The location of the NTS shown in Fig. 2a, is about 65 miles northwest of Las Vegas. A total of 26 meteorological towers were placed within the NTS to support atmospheric nuclear testing; today there are only 15 operational towers. Figure 2b shows the locations of the towers A set of four terrain following layers (10 m, 50 m, 300 m and 1000 m) was initially used to establish node locations utilizing the USGS digital elevation map. A 3-D view of an equivalent mesh generated by an h-adaptive finite element model is shown in Fig. 3a. Wind velocities obtained at the tower locations are shown in Fig. 3b. In the earlier study conducted by Pepper and Wang [24], their adaptive finite element model created a mesh consisting of 10,392 elements and 12,508 nodes.

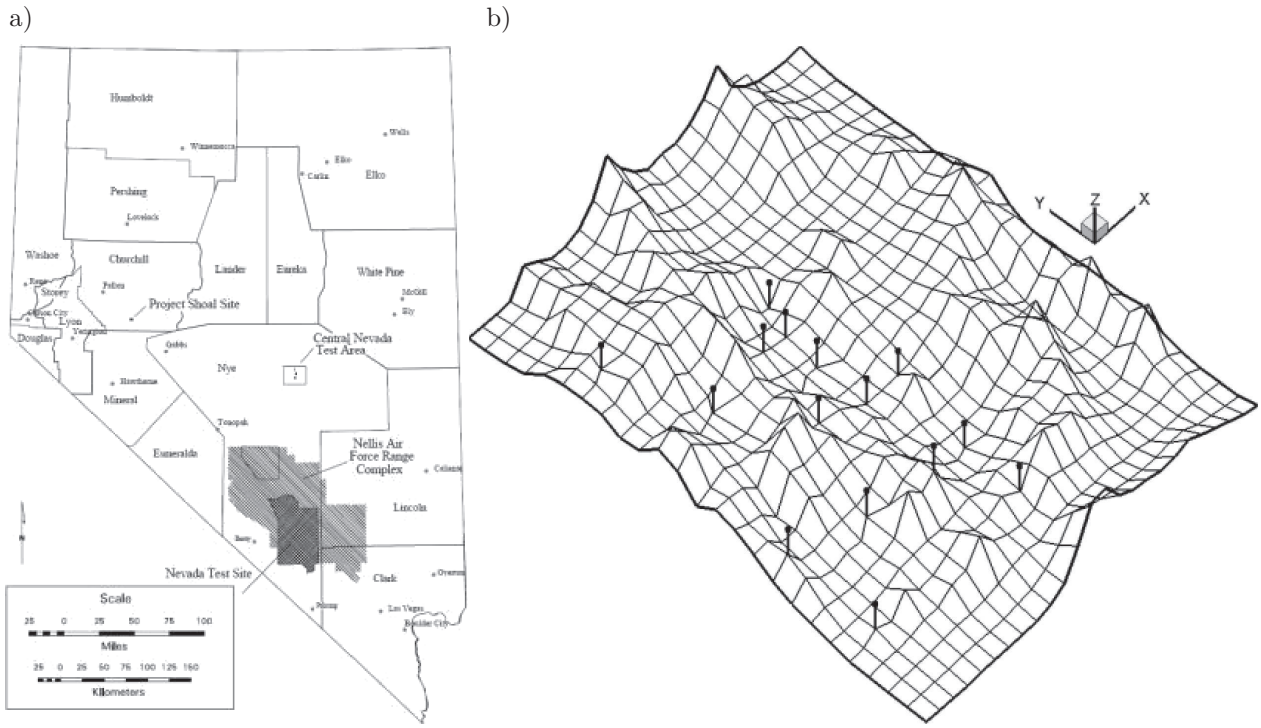

Fig. 2. a) Nevada Test Site and b) location of meteorological towers (from Pepper and Wang [24]).

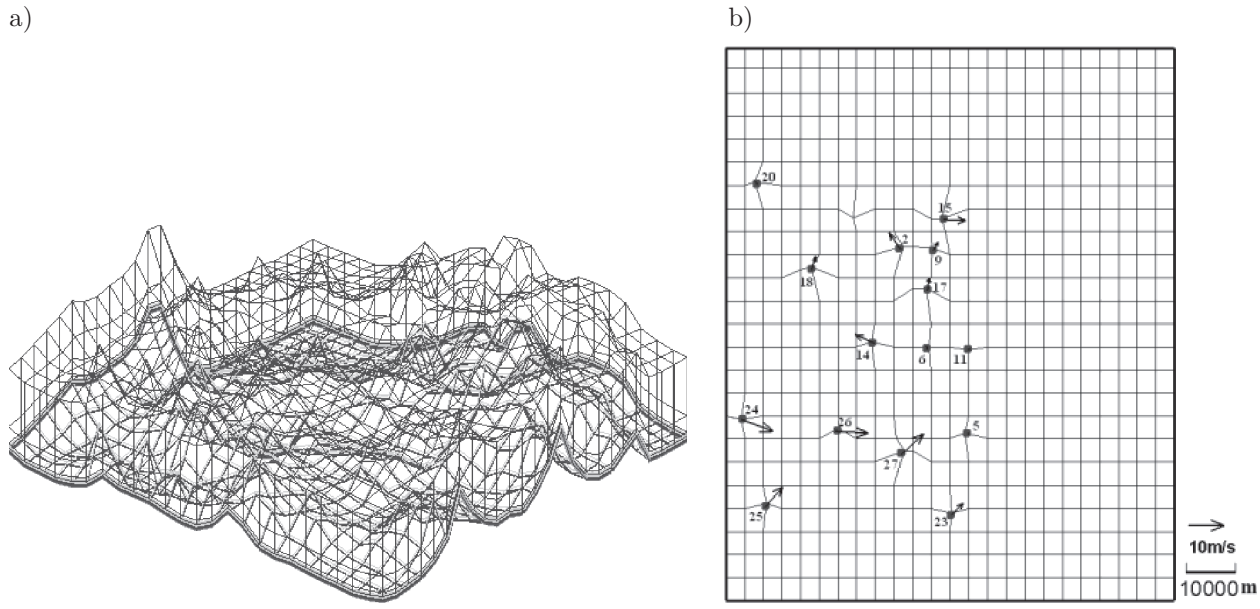

Fig. 3. a) 3-D equivalent mesh and b) measured wind velocities (from Pepper and Wang [24]).

Three-dimensional, mass consistent wind fields were constructed utilizing the data obtained from the tower network. The recorded averaged measured data for each tower utilized velocities averaged over 15 minute intervals. There are many times when many of the individual towers were offline due to equipment failure or weather extremes. Wind speeds and directions associated with the fifteen towers during this period of time are shown in Table 1. The averaged wind velocity vectors at each tower location for one period of time are shown in Fig. 3b.

Table 1. Average wind speed records of NTS towers on Jan, 1, 1993.

Tower	U [m/s]	V [m/s]
2	−3.07	4.76
5	0.13	−0.62
6	−0.27	−0.98
9	1.53	2.44
11	0.93	−0.059
14	−5.42	2.57
15	6.18	−0.35
17	0.46	3.65
18	1.22	4.06
20	0.43	−0.90
23	3.22	3.32
24	8.91	−3.25
25	4.93	5.59
26	9.20	−0.52
27	6.21	5.54

Mass consistent wind fields generated by the meshless method are compared to the h-adapted finite element results for the 10 m and 50 m levels in Figs. 4 and 5. As can be seen, the meshless results appear close in values and pattern compared with the high resolution finite element model. While both methods produce realistic wind fields, the computational work utilizing the meshless approach was significantly less, and was run using MATLAB on a PC, versus the h-adaptive finite element model that was run on a supercomputer employing FORTRAN. While other numerical schemes are commonly used to produce mass consistent, 3-D wind fields, typically finite difference

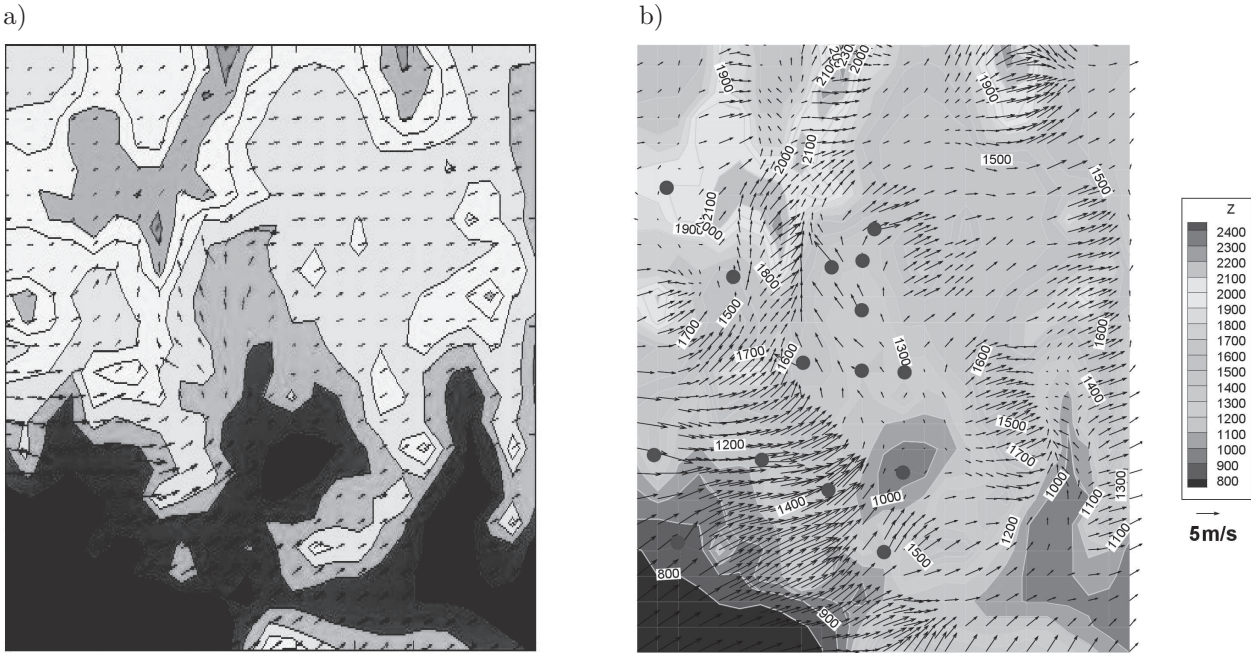

Fig. 4. a) Meshless results for 10 m level and b) hp-fem results.

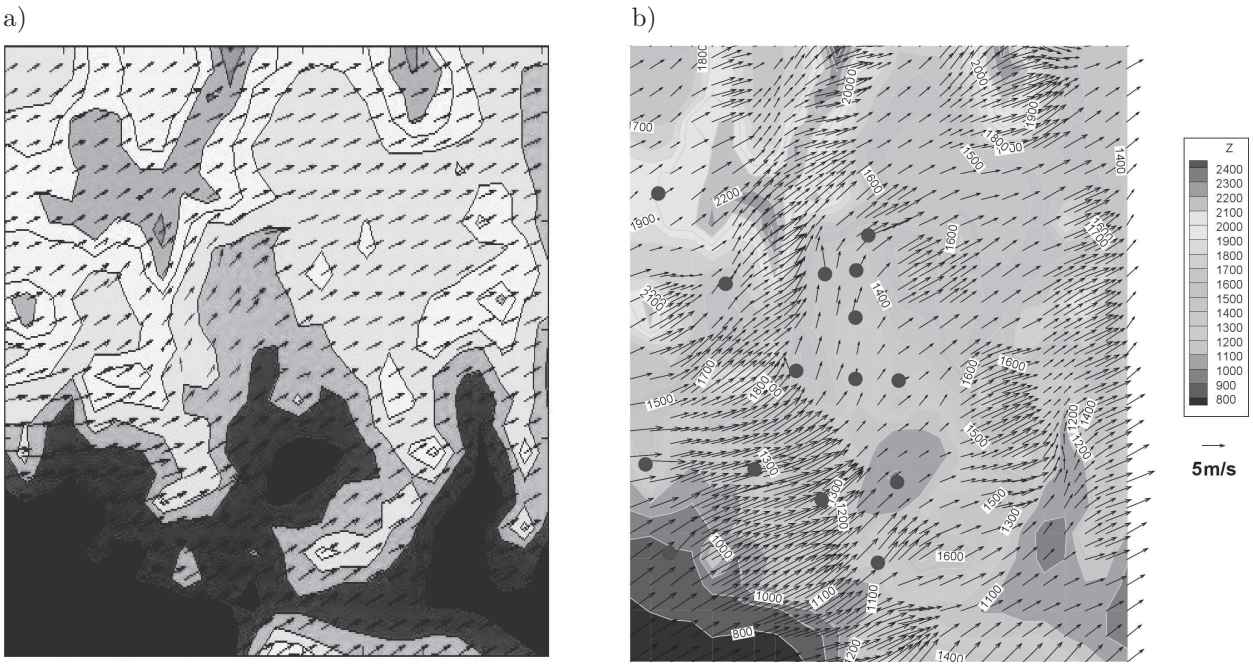

Fig. 5. a) Meshless results for 50 m level and b) hp-fem results.

or finite volume methods such schemes can be time consuming and generally demand large storage requirements [24].

5. Conclusion

A meshless method using global radial basis functions has been used to create a mass consistent, 3-D wind fields utilizing a Sasaki variational approach and sparse meteorological tower data. Wind fields are presented for the Nevada Test Site. Model results obtained with the meshless method are in good agreement with results obtained from an h-adaptive finite element model. The application of the meshless method permits the rapid construction of localized high resolution wind field estimates in regions where conventional numerical methods would require a dense, refined mesh demanding large storage and computational times. The method appears useful in refining meteorological tower locations and quickly determining potential wind turbine sites in wind energy assessment studies. A local RBF meshless approach is under development, and shows promise in reducing the overall computational effort.

References

[1] J.M. Acres. Modeling arterial blood flow using radial basis functions. MS Thesis, *University of Nevada Las Vegas*, LV, NV, p. 55, 2010.

[2] S.N. Atluri, T. Zhu. A new Meshless Local Petrov-Galerkin (MLPG) approach in computational mechanics. *Comput. Mech.*, **22**: 117–127, 1998.

[3] G.R. Balachandran, A. Rajagopal, S.M. Sivakumar. Mesh free Galerkin method based on natural neighbors and conformal mapping. *Comput. Mech.*, **42**(6): 885–905, 2009.

[4] Y. Choi, S.J. Kim. Node Generation Scheme for the Mesh-less Method by Voronoi Diagram and Weighted Bubble Packing. *Fifth US National Congress on Computational Mechanics*, Boulder, CO, 1999.

[5] M.H. Dickerson. MASCON – A mass consistent atmospheric flux model for regions with complex terrain. *J. Appl. Meteor.*, **17**: 241–253, 1978.

[6] G.E. Fasshauer. Newton iteration with multiquadrics for the solution of nonlinear PDEs. *Comput. and Math. Appl.*, **43**(3–5): 423–438, 2002.

[7] G.E. Fasshauer. *Meshfree approximation methods with MATLAB*. World Scientific Pub. Co., Singapore, p. 500, 2007.
[8] S. Finardi, G. Tinarelli, P. Faggian, G. Brusasca. Evaluation of different wind field modeling techniques for wind energy applications over complex topography. *J. Wind Eng. Ind. Aero.*, **74–76**: 283–294, 1998.
[9] R. Franke. Scattered data interpolation tests of some methods. *Math. of Comput.*, **38**: 181–200, 1982.
[10] L. Gewali, D.W. Pepper. Adaptive Node Placement for Mesh-Free Methods. *ICCES'10*, Las Vegas, NV, 2010.
[11] W.R. Goodin, G.J. McCrae, J.H. Seinfeld. An objective analysis technique for constructing three-dimensional urban-scale wind fields. *J. Appl. Meteor.*, **19**: 98–108, 1980.
[12] W.R. Goodin, G.J. McCrae, J.H. Seinfeld. A comparison of interpolation methods for sparse data: application to wind and concentration fields. *J. Appl. Meteor.*, **18**: 761–771, 1979.
[13] R.L. Hardy. Multiquadric equations of topography and other irregular surfaces. *J. of Geophy. Res.*, **176**: 1905–1915, 1971.
[14] E.J. Kansa. Multiquadrics. A scattered data approximation scheme with applications to computational fluid dynamics, II. Solutions to parabolic, hyperbolic, and elliptic partial differential equations. *Comput. and Math. Appl.*, **19**(8–9): 147–161, 1990.
[15] E.J. Kansa. Highly accurate methods for solving elliptic and parabolic partial differential equations. *WIT Transactions on Modelling and Simulation*, **39**: 5–15, 2005.
[16] T. Kitada, A. Kaki, H. Ueda, L.K. Peters. Estimation of vertical air motion from limited horizontal wind data-a numerical experiment. *Atmos. Environ.*, **17**: 2181–2192, 1983.
[17] R. Lange. A three-dimensional transport-diffusion model for the dispersal of atmospheric pollutants and its validation against regional tracer studies. *J. Appl. Meteor.*, **17**: 241–256, 1978.
[18] X.Y. Li, S.H. Teng, A. Ungor. Generating a Good Quality Point Set for the Mesh-less Methods. *Computer Modeling in Engineering Sciences (CMES)*, **1**(1): 10–17, 2000.
[19] G.R. Liu. *Mesh Free Methods: Moving beyond the Finite Element Method*. CRC Press, Boca Raton, 2003.
[20] R. Mathur, L.K. Peters. Adjustment of wind fields for application in air pollution modeling. *Atmos. Environ.*, **24**: 1095–1106, 1990.
[21] G. Montero, N. Sanin. 3-D modeling of wind field adjustment using finite differences in a terrain conformal coordinate system. *J. Wind Eng. Ind. Aero.*, **89**: 471–488, 2001.
[22] G.E. Montero, R. Rodrıguez, J.M. Montenegro, J.M. Escobar, J.M. Gonzalez-Yuste. Genetic algorithms for an improved parameter estimation with local refinement of tetrahedral meshes in a wind model. *Adv. Eng. Software*, **36**: 3–10, 2005.
[23] D.W. Pepper. A Finite Element Model for Calculating 3-D Wind Fields over Vandenberg Air Force Base. *29th AIAA Aerospace Sciences Meeting*, Jan. 7–10, Reno, NV, Amer. Institute Aeronaut. Astronaut., AIAA pp. 91–0451, 1991.
[24] D.W. Pepper, X. Wang. An *h*-adaptive finite-element technique for constructing 3D wind fields. *J. Appl. Meteor. and Climat.*, **48**: 580–599, 2009.
[25] D.W. Pepper, X. Wang. Application of an *h*-adaptive FEM for wind energy assessment in Nevada. *Renew. Energy*, **32**: 1705–1722, 2007.
[26] R. Pielke. *Mesoscale meteorological modeling*. Academic Press, New York, N.Y., pp. 612, 1984.
[27] C.F. Ratto, R. Festa, C. Romeo, O.A. Frumento, M. Galluzzi. Mass-consistent models for wind fields over complex terrain: the state of the art. *Environ. Software*, **9**: 247–268, 1994.
[28] C.M.C. Roque, A.J.M. Ferreira. Numerical experiments on optimal shape parameters for radial basis functions. *Num. Meth. Part. Diff. Eqns.*, **26**(3): 675–689, 2009.
[29] Y. Sasaki. An objective analysis based on the variational method. *J. Meteor. Soc. Japan*, **36**: 77–88, 1958.
[30] J.T. Schaefer, C.A. Doswell III. On the interpolation of a vector field. *Mon. Weather Rev.*, **107**: 458–476, 1979.
[31] C.A. Sherman. A mass-consistent model for wind field over complex terrain. *J. Appl. Meteor.*, **17**: 312–319, 1978.
[32] R. Trobec, G. Kosec, M. Sterk, B. Sarler. Comparison of local weak and strong form meshless methods for 2-D diffusion equation. *Engr. Analysis with Boundary Elements*, **36**(3): 310–321, 2012.
[33] T.T. Warner, R.R. Fizz, N.L. Seaman. A comparison of two types of atmospheric transport models – use of observed winds versus dynamically predicted winds. *J. Climate Appl. Meteor.*, **22**, 394-406, 1983.
[34] J. Waters, D.W. Pepper. Global versus localized RBF meshless methods for solving incompressible fluid flow with heat transfer. *Num. Heat Transfer, Part B*, **68**(3): 185–203, 2015.
[35] G. Yao, S. Islam, B. Sarler. Assessment of global and local meshless methods based on collocation with radial basis functions for parabolic partial differential equations in three dimensions. *Engr. Analysis with Boundary Elements*, **36**(11): 1640–1648, 2012.